Bioconjugate Chemistry

Article

pubs.acs.org/bc

PEGylated Fluorescent Carbon Nanoparticles for Noninvasive Heart Imaging

Shaobo Ruan,[†] Jingyu Wan,[†] Yao Fu,[†] Ke Han,[†] Xiang Li,[†] Jiantao Chen,[†] Qianyu Zhang,[†] Shun Shen,[‡] Qin He,[†] and Huile Gao*[,†]

[†]Key Laboratory of Drug Targeting and Drug Delivery Systems, West China School of Pharmacy, Sichuan University, No. 17, Block 3, Southern Renmin Road, Chengdu 610041, China

[‡]Key Laboratory of Smart Drug Delivery (Fudan University), Ministry of Education; Department of Pharmaceutics Sciences, School of Pharmacy, Fudan University, 826 Zhangheng Road, Shanghai, 201203, China

ABSTRACT: Fluorescent carbon nanoparticles (CNP) have gained much attention due to their unique fluorescent properties and safety. In this study, we evaluated the potential application of CNP and PEGylated CNP (PEG-CNP) in noninvasive heart imaging. CNP was prepared by hydrothermal treatment of silk. The particle size and zeta potential of CNP were 121.8 nm and −3.7 mV, respectively, which did not change significantly after PEGylation with a PEG density of 4.43 ± 0.02 μg/mg CNP. FTIR and XPS showed that CNP possessed several functional groups, such as −COOH, −OH, and NH_2, which could be utilized for PEGylation and other modifications. CNP displayed strong blue fluorescence after excitation at the wavelength of 375 nm. PEG-CNP displayed better serum stability compared to CNP. The hemolysis rate of PEG-CNP was lower than that of CNP, suggesting PEGylation could enhance the hemocompatibility of CNP. Both CNP and PEG-CNP showed higher uptake capacity by H9c2 cells (a heart cell line) than that by human umbilical vein endothelial cells (HUVEC), suggesting the particles tend to be selectively taken up by heart cells. Both CNP and PEG-CNP were proven to be taken up through endosome-mediated pathway, and the colocalization of nanoparticles with mitochondria was also observed. In vivo results demonstrated that CNP could target heart with much higher fluorescent intensity than liver and spleen. Although PEGylation could decrease the distribution in heart, it remained high for PEG-CNP. In conclusion, CNP could be used for heart imaging, and moreover, PEGylation could improve the stability and biocompatibility of CNP.

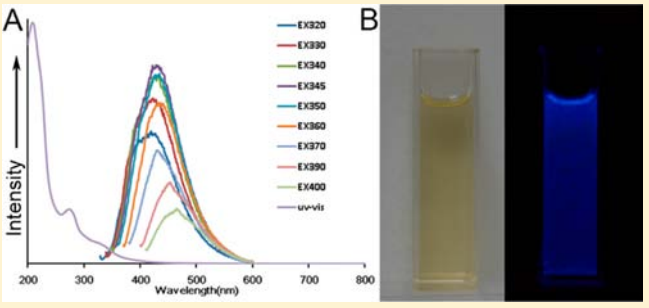

INTRODUCTION

Fluorescent quantum dots have attracted much attention owing to their colorful fluorescent properties which can be widely used in disease or cell detection. However, the application is limited by the potential toxicity caused by the presence of heavy metals in the quantum dots.[1] As newly emerged fluorescent dots, carbon based nitrogen-doped nanospheres (CNP) represent a promising alternative because of the following properties: photoluminescence, low photobleaching, no optical blinking, low toxicity, and good biocompatibility. Thus, CNP can be applied in biological systems as a superior alternative to traditional organic dyes and quantum dots.[2−8]

At present, most reports are focused on the simple methods to develop CNP with excellent characteristics from different materials, such as cocoon silk, chitosan, and orange juice.[3,9,10] However, its potential for in vivo application remains unknown. In this study, CNP was prepared from cocoon silk using a simple one-step method. The fluorescent property and surface functional groups were evaluated to determine if CNP could be used for cell or organ imaging.

For biological applications, the stability and safety of CNP was a major concern.[11,12] However, as far as we know, there were rarely discussions on the stability and safety of CNP, although cytotoxicity was often evaluated in previous studies.[9,13] Thus, in this study, not only cytotoxicity, but also hemocompatibility and serum adsorption were evaluated to determine the safety and stability of CNP. As a commonly used method to improve the stability and safety of materials,[14] PEGylation was also applied in the current study and was used as a control for bare CNP.

The heart is one of the most important organs for human beings. Correspondingly, heart-related disease is one of the most common diseases. Normally, heart imaging is performed using magnetic resonance imaging, computed tomography, and ultrasound imaging.[15,16] According to our experiments, CNP showed strong accumulation in the heart, which has not been reported yet. Thus, in this study, we evaluated the potential of CNP and PEGylated CNP (PEG-CNP) in heart imaging.

Received: February 17, 2014
Revised: May 9, 2014
Published: May 22, 2014

   dx.doi.org/10.1021/bc5001627 | *Bioconjugate Chem.* 2014, 25, 1061−1068

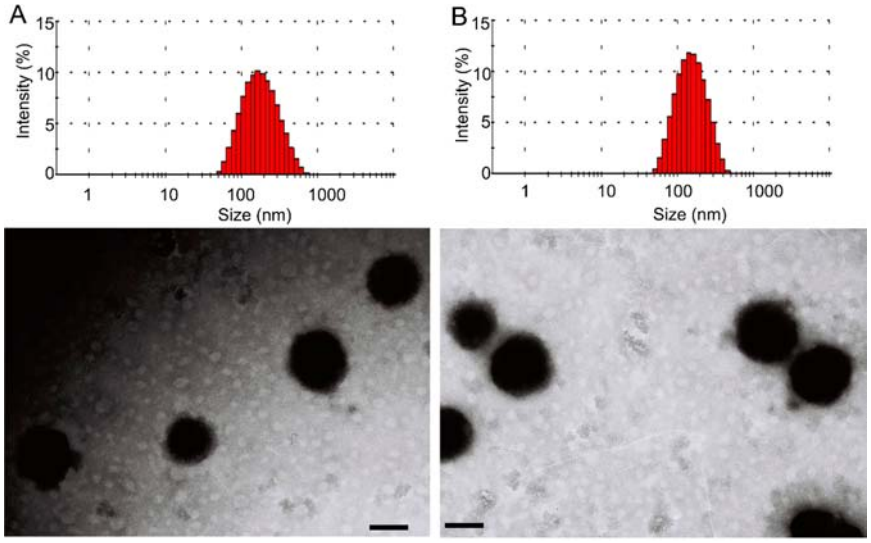

Figure 1. (A) DLS data and TEM image of CNP; (B) DLS data and TEM image of PEG-CNP; bar represents 100 nm.

RESULTS AND DISCUSSION

Characterization. The hydrated CNP particle displayed an average size of 121.8 nm with a polydispersity index of 0.276. TEM showed that CNPs were spherical with uniform size which indicated good dispersion (Figure 1A). Zeta potential of CNP was −3.7 mV, which was mainly due to the carboxyl units on the surface of CNP and was useful for maintaining stability in aqueous solution. After modification, the density of PEG was 4.43 ± 0.02 μg/mg CNP. Modification with PEG led to an increase in particle size to 139.6 nm (Figure 1B), with a zeta potential of −7.82 mV, which was a result of the shielding of PEG. The PEG density is crucial to prevent the opsonin adsorption, because only PEG with intensity high enough could form a brush configuration rather than mushroom.[17,18] However, the density of CNP was unknown, which made it impossible to calculate the exact number of PEG per particle. Alternatively, serum stability was investigated to elucidate the protein adsorption property of both CNP and PEG-CNP.

In the FTIR analysis of CNP (Figure 2A), the following vibrations were observed: stretching vibrations of C−OH at 3424 cm^{-1}, asymmetric stretching vibrations of C−NH−C at 1114 cm^{-1}, stretching vibrations of C═C at 1633, 1513, and 1463 cm^{-1}, indicating that the structures of CNP might contain polycyclic aromatic and aromatic CN groups.[3,19,20] PEG-CNP was also characterized by FTIR. A typical peak at 1098 cm^{-1} was observed (Figure 2B), contributing to the stretching vibration of C−O−C, while the peak at 3424 cm^{-1} in the spectrum of CNP was obviously changed in the spectrum of PEG-CNP. In the FTIR spectrum of NH_2−PEG, a typical peak was observed at 1640 and 2921 cm^{-1} (Figure 2C), contributing to the vibration of −C−C−/−NH_2 and −CH_2−, respectively. Combining the differences in particle size and FTIR spectrum, it is suggested that the PEG has been modified onto the CNP.

Surface states of the CNP were further characterized by XPS. The XPS spectrum showed three peaks at 284.6, 400.7, and 530.7 eV (Figure 2D), contributed by C_{1s}, N_{1s}, and O_{1s} respectively. The C_{1s} spectrum (Figure 2E) displayed four peaks at 284.56, 285.7, 286.9, and 287.82 eV, which were attributed to C−C, C−N, C−O, and C═N/C═O, respectively.[21] The N_{1s} spectrum (Figure 2F) showed three peaks at 399.9, 400.7, and 401.23 eV, which were contributed by the C−N−C, N−C, and N−H bands, respectively.[22] The O_{1s} spectrum (Figure 2G) exhibited two peaks at 530.68 and 531.45 eV, which were attributed to C═O and C−OH/C−O−C groups, respectively.[3] These results demonstrated that the surface of CNP possessed plentiful oxygen and nitrogen functional groups, which was consistent with previous studies and useful for further modification.[3,21] Similar peaks were observed in the spectrum of PEG-CNP (Figure 2I, J, and K) and the ratio of C in the surface of PEG-CNP was higher than that of CNP (Figure 2H), contributing to the higher C ratio in PEG (Figure 2L), suggesting that PEG was successfully anchored onto CNP.

Fluorescent Property. Figure 3 displayed the optical properties of the CNP. In the UV absorption curve, there were obvious absorption peaks at 208 and 273 nm (Figure 3A), which were the typical properties of fluorescent carbon dots. When excited at 345 nm, CNP displayed strong blue photoluminescence with a peak at 434 nm (Figure 3B). Increasing the excitation wavelength led to a red-shift of the emission peak, which was attributed to the synergistic effect of the core and the surface of CNP.[3] At room temperature, CNP showed a clear yellow state and could be excited into strong blue color under UV light (365 nm, Figure 3B). The fluorescent properties enabled CNP with potential applications in bioimaging. The relatively quantum yield was 34.2%, which was consistent with previous results.

Stability. For potential in vivo application, protein adsorption is one of the major concerns that needed to be addressed since protein coronas were often formed on the surface of nanoparticles and altered their stability and in vivo behavior.[23] After incubation with different concentrations of human serum, the absorption of CNP at 560 nm was obviously increased, which was positively related to the incubation time (Figure 4), suggesting that CNP could interact with serum proteins and lead to protein adsorption. PEGylation was shown to reduce protein adsorption onto CNP when incubated with 50% human serum. The addition of PEG enhanced the hydrophilicity of CNP, preventing the interaction of CNP with proteins, especially the interaction between CNP and opsonin. Protein adsorption thus delayed and decreased, which may benefit the in vivo application of CNP by avoiding RES recognization and elimination.[17,24] Despite the sharp increase in the absorbance of PEG-CNP in serum from 8 to 12 h, the

dx.doi.org/10.1021/bc5001627 | Bioconjugate Chem. 2014, 25, 1061−1068

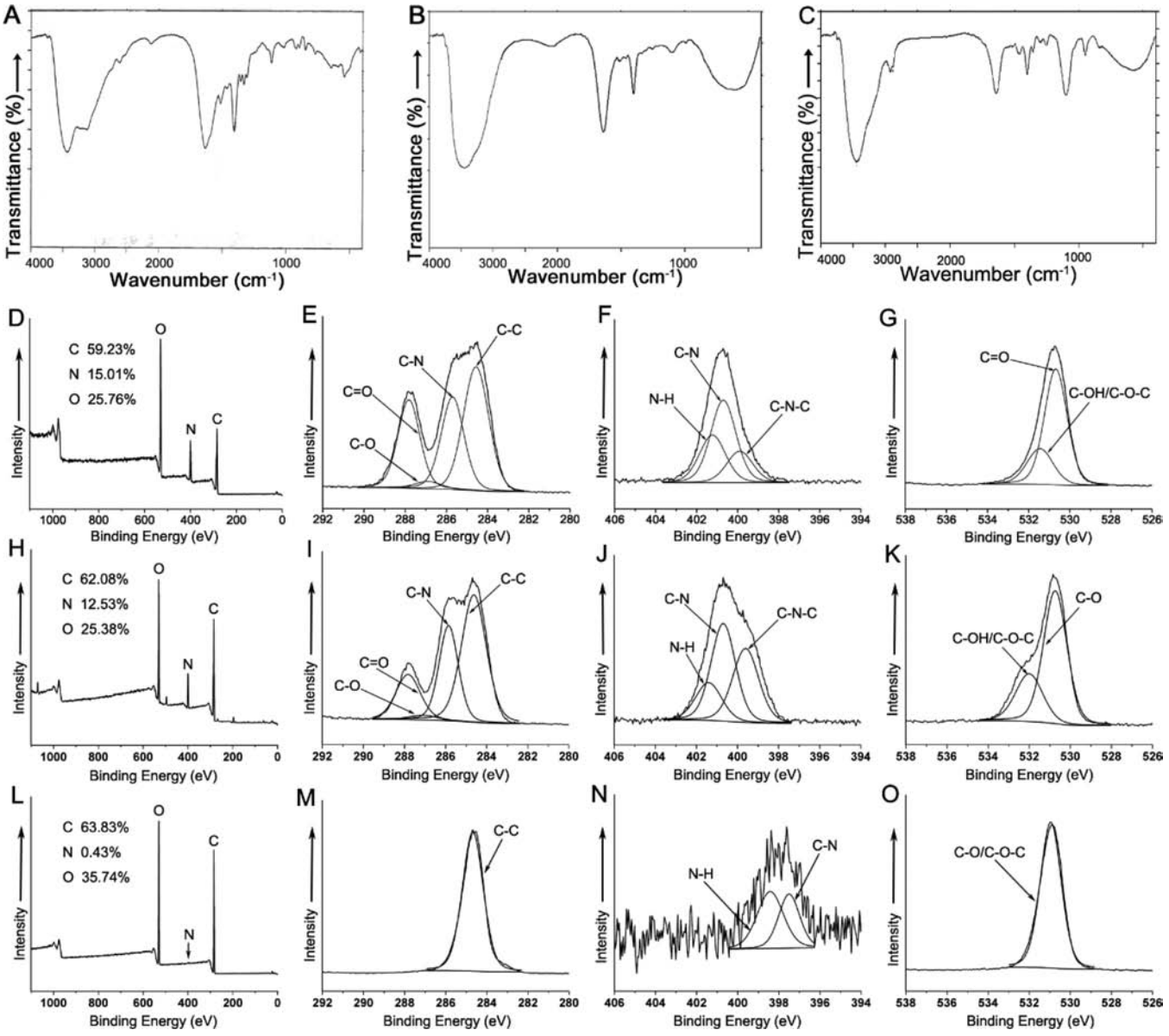

Figure 2. (A) FT-IR spectrum of CNP. (B) FT-IR spectrum of PEG-CNP. (C) FT-IR spectrum of NH_2−PEG. (D) XPS survey spectrum of CNP. (E) XPS C_{1s} spectrum of CNP. (F) XPS N_{1s} spectrum of CNP. (G) XPS O_{1s} spectrum of CNP. (H) XPS survey spectrum of PEG-CNP. (I) XPS C_{1s} spectrum of PEG-CNP. (J) XPS N_{1s} spectrum of PEG-CNP. (K) XPS O_{1s} spectrum of PEG-CNP. (L) XPS survey spectrum of NH_2−PEG. (M) XPS C_{1s} spectrum of NH_2−PEG. (N) XPS N_{1s} spectrum of NH_2−PEG. (O) XPS O_{1s} spectrum of NH_2−PEG.

sharp increase of CNP appeared earlier, from 2 to 8 h. These results demonstrated that PEG is useful for improving serum stability of CNP. However, as demonstrated previously, PEGylation could not eliminate protein adsorption completely.[25] When protein adsorption achieved a threshold, the particles tend to aggregate, leading to a sharp increase in absorption. However, for in vivo imaging, the concentration of PEG-CNP decreased as time increased, thus making it difficult for PEG-CNP to aggregate.

Hemocompatibility. Hemocompatibility is another concern for in vivo application because poor hemocompatibility could lead to acute toxicity to bodies. The hemocompatibility was time- and concentration-dependent. Increasing both incubation time of CNP with red blood and concentration of CNP could significantly elevate the hemolysis rate (Figure 5A and B), which was consistent with previous studies.[26] However, PEGylation could significantly decrease the hemolysis rate, which was 72.4% that of CNP after 24 h incubation. The differences in hemolysis rate could be directly observed (Figure 5C). Additionally, the hemolysis rate was also concentration-related, as elevated concentration of CNP and PEG-CNP could significantly increase the hemolysis rate. At a concentration of 1 mg/mL, the hemolysis rate of CNP could decrease from 20.2% to 13.7% after PEGylation. However, for traditional quantum dots, such as CdTe, obvious hemolysis (19.4%) could be observed after 4 h incubation of 120 μg/mL of these dots with red blood cells.[27] Covering with glutathione or silica shell could improve the hemocompatibility.[27,28] The above results suggested that PEGylation could effectively improve the hemocompatibility of CNP, making PEG-CNP a promising diagnosis probe for in vivo application.

Cytotoxicity of CNP. To evaluate the cytotoxicity of CNPs, HUVEC and H9c2 cells were incubated with serial concentrations of CNP for 24 h. As shown in Figure 6, the

dx.doi.org/10.1021/bc5001627 | Bioconjugate Chem. 2014, 25, 1061−1068

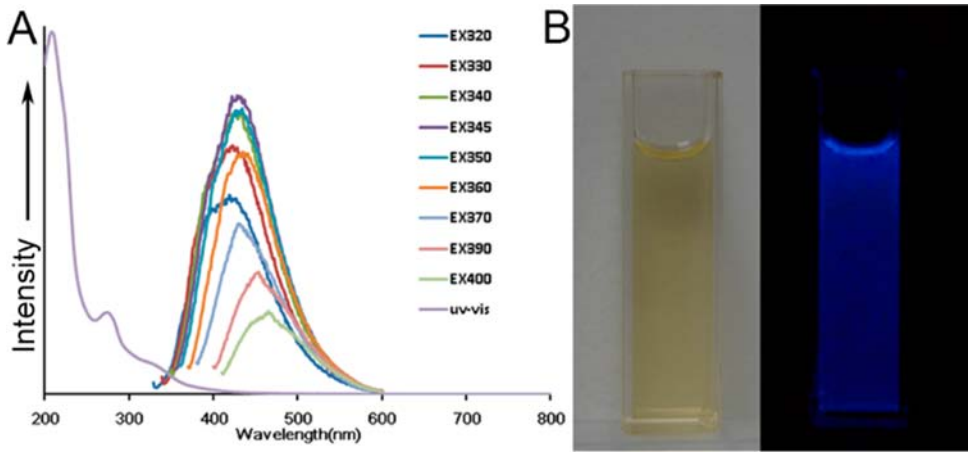

Figure 3. (A) Absorption spectrum at UV−vis and emission spectrum at different excitation wavelengths of CNP. (B) Photograph of CNP excited by daylight and a 365 UV lamp.

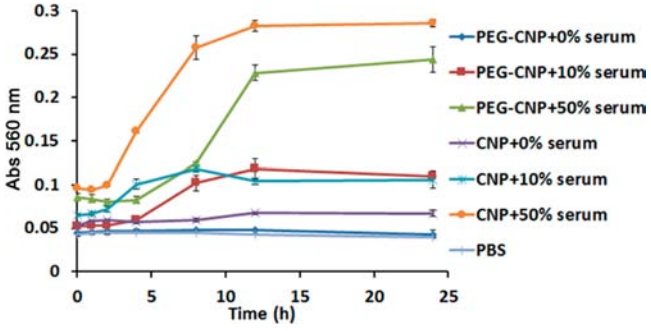

Figure 4. Stability of CNP and PEG-CNP in different concentrations of human serum.

cell viability of HUVEC was not obviously changed between controls and cells treated with CNP and PEG-CNP at a concentration as high as about 1 mg/mL, but this concentration of PEG-CNP could obviously inhibit the proliferation of H9c2 cells. Although 8 mg/mL of CNP and PEG-CNP could decrease the cell viability of both cells to approximately 60% to 80% compared to the control, the concentration was much higher than that used for imaging (100 μg/mL for in vitro imaging and 5 mg/kg for in vivo imaging), suggesting that the cytotoxicity of CNP and PEG-CNP was relatively low. However, at some concentrations, the cytotoxicity of PEG-CNP was higher than that of CNP, which may be because of the remaining EDC and NHS that were used for CNP activation and PEG conjugation.

Cell Uptake and Subcellular Localization. Although both HUVEC and H9c2 cells could take up CNP, the uptake by H9c2 cells was much higher than that by HUVEC (Figure 7 and Figure 8), suggesting the selectivity of CNP to H9c2 cells.

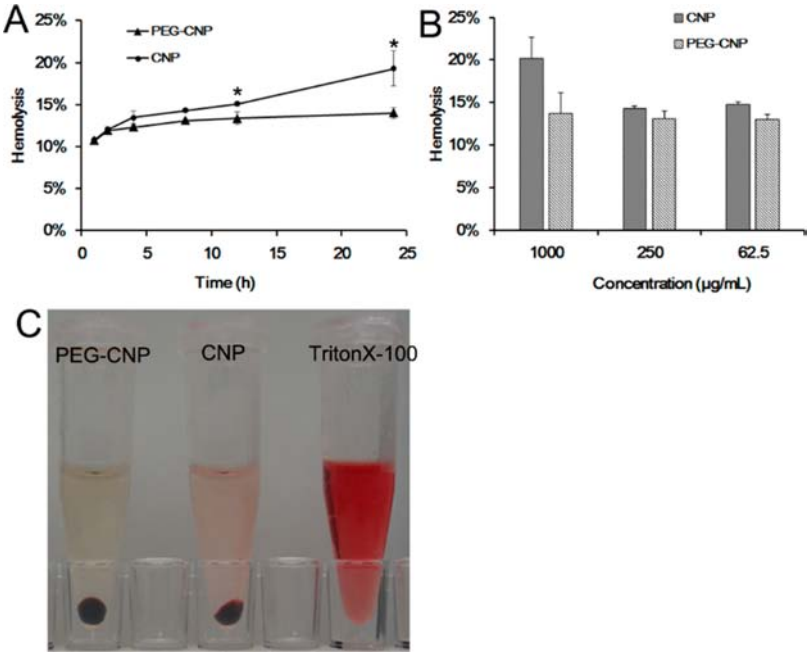

Figure 5. (A) Hemolysis rate of 250 μg/mL of CNP and PEG-CNP incubated with 2% red blood cells for various times. (B) Hemolysis rate of different concentrations of CNP and PEG-CNP incubated with 2% blood red cells for 8 h. (C) Hemolysis of 250 μg/mL of CNP and PEG-CNP incubated with 2% blood red cells for 24 h.

dx.doi.org/10.1021/bc5001627 | *Bioconjugate Chem.* 2014, 25, 1061−1068

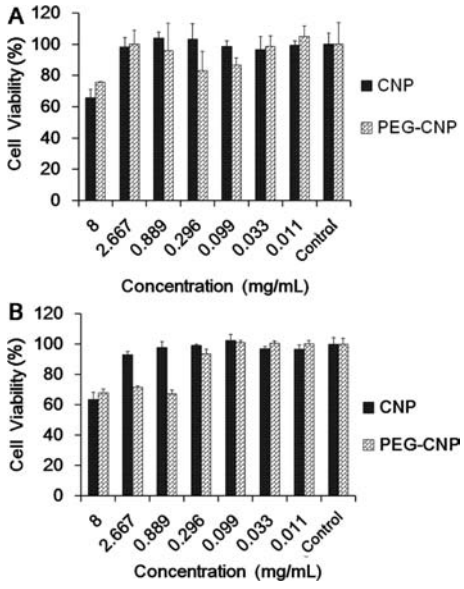

Figure 6. Cell viability of HUVEC (A) and H9c2 cells (B) treated with different concentrations of CNP and PEG-CNP for 24 h.

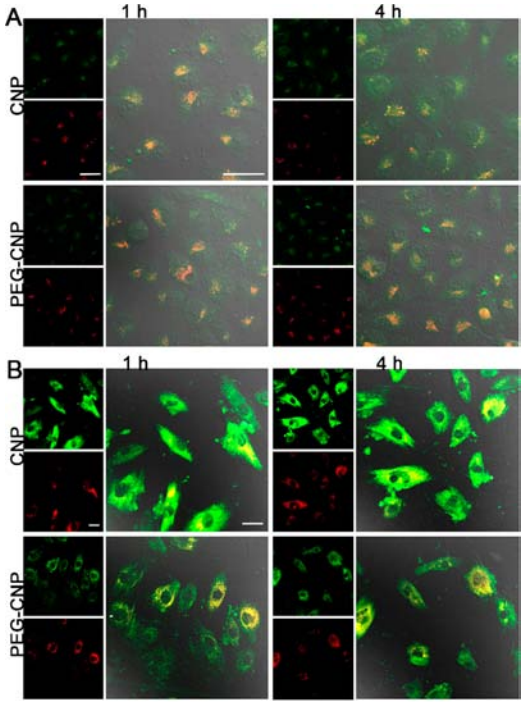

Figure 7. HUVEC (A) and H9c2 (B) cell uptake and subcellular localization of CNP and PEG-CNP with endosomes. Bar represents 40 μm.

PEG-CNP displayed lower uptake amount by both cells than the uptake of CNP, owing to the hindering effect of PEG. However, the uptake of PEG-CNP by H9c2 cells was still higher than that by HUVEC, suggesting PEG-CNP could be used for heart imaging.

In both cell lines, CNP colocalized with endosomes after 1 h incubation (Figure 7), suggesting endosomes were involved in the uptake process. Increasing the incubation to 4 h decreased the colocalization of CNP with endosomes in HUVEC cells, which is mostly likely due to the escape of CNP from endosomes. However, in H9c2 cells, the colocalization at 4 h

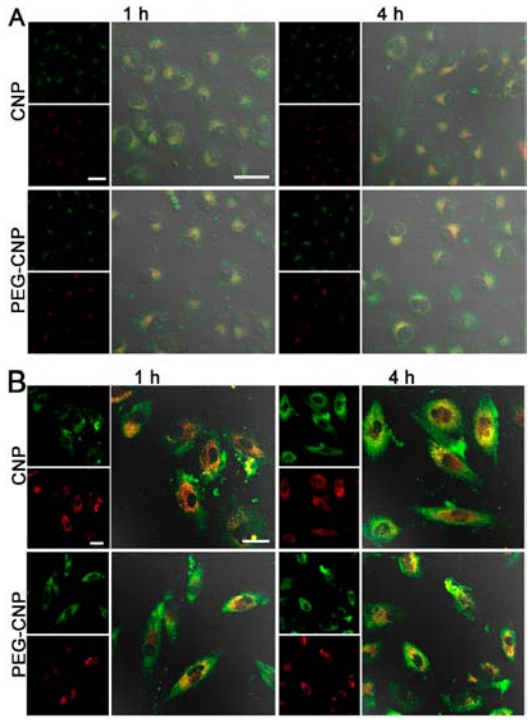

Figure 8. HUVEC (A) and H9c2 (B) cell uptake and subcellular localization of CNP and PEG-CNP with mitochondria. Bar represents 40 μm.

remained the same as that at 1 h, suggesting CNP could not escape from endosomes in H9c2 cells. Additionally, PEGylation could increase the colocalization with endosomes and delay the escape from endosomes, which should be taken into consideration when using PEG-CNP for constructing drug delivery systems.

Moreover, CNP and PEG-CNP showed high colocalization with mitochondria (Figure 8), which may be useful for mitochondria-targeted delivery. However, to achieve this purpose, nanoparticles were often functionalized with a mitochondria-targeted sequence.[29] Thus, further investigations are required to interpret the high colocalization of CNP/PEG-CNP with mitochomdria.

Tissue Distribution. To further elucidate the heart imaging potency of PEG-CNP, whole body distribution imaging of CNP and PEG-CNP was carried out through tissue slicing 2 h after i.v. injection of CNP or PEG-CNP through tail vein at a dose of 100 mg/kg. CNP distributed in the heart with the highest intensity among all the organs (Figure 9). Even the distribution in liver and spleen was lower than that in heart, suggesting that CNP possessed high potency in heart imaging. To improve the compatibility, CNP was covered with PEG. Although the distribution of PEG-CNP in heart was relatively lower than that of CNP, it was still higher than the distribution of PEG-CNP in lung, liver, and brain. The reasons for the increased distribution in spleen, kidney, and liver might be that PEGylation decreased the distribution in heart, brain, and lung but increased the blood circulation time, thus providing more opportunities to be captured by organs that eliminated the foreign materials. The decreased distribution of PEG-CNP in brain and lung may improve the safety of PEG-CNP. For most nanosized particles, the distribution in liver and spleen was often higher than that in other organs/tissues, even after modification with specific targeting ligands. In addition, the

dx.doi.org/10.1021/bc5001627 | Bioconjugate Chem. 2014, 25, 1061−1068

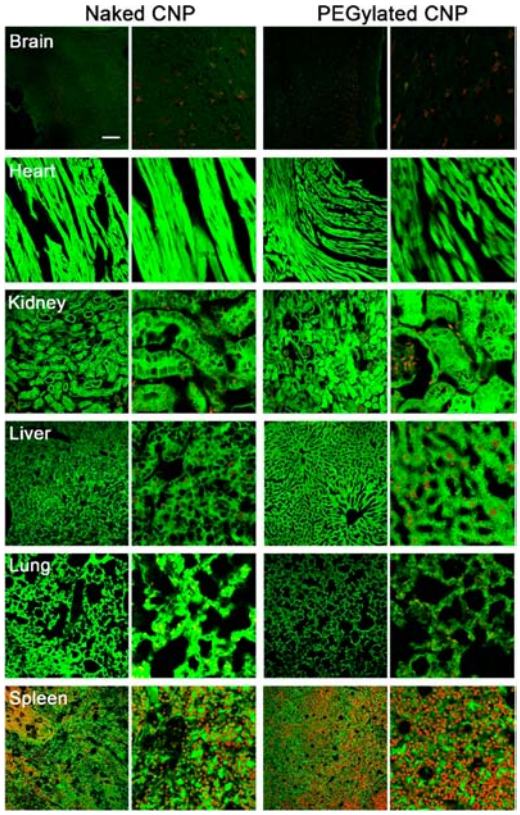

Figure 9. Distribution of CNP and PEG-CNP in various organs of mice; enlarged (4×) pictures were also shown at the right of the original pictures. Nuclei were stained with PI and the bar represents 100 μm.

distribution in heart was often lower than in other organs except brain.[30,31] Thus, it was interesting that CNP and PEG-CNP could distribute into heart. Currently, heart diseases, especially various forms of amyloidosis and cardiomyopathy, are huge threats for human beings. Early and accurate diagnosis of these cardiac amyloidoses is essential but often delayed.[32] CNP may serve as a potential diagnosis probe for these diseases, which needed to be further evaluated.

CONCLUSION

In this study, we evaluated the potential application of CNP and PEGylated CNP (PEG-CNP) in noninvasive heart imaging. CNP was prepared by hydrothermal treatment of silk. FTIR and XPS showed that CNP possessed several functional groups, such as −COOH, −OH, and $-NH_2$, which could be utilized for PEGylation and other modifications. CNP displayed strong blue fluorescence at the excitation wavelength of 375 nm. After PEGylation, PEG-CNP displayed improved stability and hemocompatibility compared to CNP. In vitro cellular uptake study demonstrated that both CNP and PEG-CNP showed higher uptake intensity by H9c2 cells than that by HUVEC. Both CNP and PEG-CNP were taken up through endosome-mediated pathway displaying good colocalization with mitochondria. In vivo results demonstrated that CNP could target the heart, in which the fluorescent intensity was much higher than that in other organs, even liver and spleen. Although PEGylation could decrease the distribution in the heart, PEG-CNP still showed high fluorescent intensity in the heart, suggesting that CNP could be used for heart imaging while PEGylation could improve the stability and biocompatibility of CNP.

MATERIALS AND METHODS

Materials. *N*-(3-(Dimethylamino)propyl)-*N*′-ethylcarbodiimide hydrochloride (EDC) and *N*-hydroxy-succinimide (NHS) were purchased from Sigma (Saint Louis, MO, USA). PI was obtained from Beyotime (Haimen, China). Amino poly(ethylene glycol) (NH_2−PEG, MW = 5000) was purchased from Seebio Biotech, Inc. (Shanghai, China). HUVEC was purchased from the Institute of Biochemistry and Cell Biology, Shanghai Institutes for Biological Sciences, Chinese Academy of Sciences (Shanghai, China). H9c2 was kindly donated by Dr. Lilong Pan (School of Pharmacy, Fudan University). Plastic cell culture dishes and plates were obtained from Wuxi NEST Biotechnology Co. Ltd. (Wuxi, China). Dulbecco's Modified Eagle Medium (high glucose) cell culture medium (DMEM) and FBS were obtained from Life Technologies (Grand Island, NY, USA).

BALB/c nude mice (male, 4−5 weeks, 18−22 g) were obtained from the Shanghai Lab. Animal Research Center (Shanghai, China) and maintained under standard housing conditions. All animal experiments were carried out in accordance with protocols evaluated and approved by the ethics committee of Sichuan University.

Preparation of CNP and PEG-CNP. Cocoon silk were treated in boiled 5% Na_2CO_3 for 1 h to remove the contamination; thus, pure silk could be reserved. After washing with deionized water 4 times to remove the Na_2CO_3, 1 g of the pure silk was added into the reaction kettle (capacity = 50 mL) that contained 10 mL of deionized water. The kettle was put into an oven set at 200 °C. After 72 h incubation, CNP could be obtained. For PEG conjugation, carboxyl units on the surface of the CNP solution (20 mg/mL) were activated by EDC and NHS in PBS for 0.5 h. Then, NH_2−PEG (80 μg/mL) was added in the solution and stirred for 2 h. The unconjugated PEG was removed by 12 h of dialysis (cutoff size = 10 kDa).

Characterization of CNP and PEG-CNP. The hydrated diameter and zeta potential were determined by a Malvern Zetasizer (Malvern, NanoZS, UK). The morphology was captured by transmission electronic microscopy (TEM) (JEM 100CX, JEOL, Japan). To determine the surface density of PEG, the unconjugated PEG was removed by dialysis and recovered by freeze−drying. Then the unconjugated PEG was dissolved and determined by barium chloride method. Briefly, 0.6 mL of PEG contained solution was added with 1.2 mL of 5% barium chloride. After reaction, 60 μL of 0.025 mol/L I_2 solution was added and the absorbance at 385 nm was determined. Fluorescence spectroscopy was evaluated by a Shimadzu RF-5301PC spectrofluorophotometer. UV−vis spectra scanning dispersed in water were determined on a Varian Cary 100 conc UV−vis spectrophotometer. Fourier transform infrared (FTIR) spectra were determined on a Bruker Vector22 spectrometer (Germany) using spectroscopic grade KBr. X-ray photoelectron spectroscopy (XPS) experiments were performed on an AXIS Ultra DLD (Kratos UK) with Mg Kα radiation ($h\nu$ = 1486.6 eV), with a chamber pressure of 2.2 × 10−9 Torr. The source power and high voltage was set at 150 W and 15 kV, and pass energies of 40 eV for survey scans was used. The analysis spot size was 300 × 700 μm^2. The data was analyzed by PHI-MATLAB software with C 1s = 284.6 eV as a benchmark for the binding energy correction. Fluorescence

dx.doi.org/10.1021/bc5001627 | *Bioconjugate Chem.* 2014, 25, 1061−1068

quantum yields were evaluated using a RF-5301PC spectrofluorophotometer (Shimadzu, Japan).

Stability of CNP and PEG-CNP. The stability of CNP and PEG-CNP was evaluated in PBS with different concentrations of FBS. CNP and PEG-CNP were suspended in 0%, 10%, 50%, or 90% FBS and incubated in a 37 °C incubator. The absorption at 560 nm were determined by a microplate reader (Multiskan MK3, Thermo, USA) at 0, 1, 2, 3, 4, 6, 8, 12, and 24 h.

Hemocompatibility of CNP and PEG-CNP. Whole blood was collected from mice using heparin as anticoagulant. After centrifugation at 1500 rpm for 5 min, the red blood cells were resuspended in PBS at the final density of 2%. Different concentrations of CNP were added into cell suspension and were incubated at 37 °C for 60 min. The absorption at 560 nm was determined by a microplate reader (Multiskan MK3, Thermo, USA). PBS was used as negative control while 1% of Triton X-100 was used as positive control.

Cytotoxicity of CNP. HUVEC and H9c2 cells were seeded into a 96-well plate at a density of 2×10^4 cells/mL. After 24 h, each well was added with CNP and PEG-CNP at a series of concentrations and incubated for another 24 h. Then 20 μL of MTT solution (5 mg/mL in PBS) was added into each well and cells were further incubated for 4 h under 37 °C. Then the media was removed and cells were dissolved by 150 mL dimethyl sulfoxide. The absorbance at 490 nm was measured by a microplate reader (Thermo Scientific Varioskan Flash, USA).

Cellular Uptake and Subcellular Localization. HUVEC and H9c2 cells were seeded into coverslip-contained plate at a density of 1×10^5 cells/mL. After 2 days incubation, cells were treated with 100 μg/mL of CNP in FBS-free DMEM for 1 or 4 h. Thirty min prior to fixation, LysoTracker Red or MitoTracker Red were added into the wells and incubated for 30 min. After three PBS washes, samples were fixed by 4% paraformaldehyde, and fluorescent distribution in cells was observed by a confocal microscope (LSM710, Carl Zeiss, Germany).

Tissue Distribution. For in vivo evaluation, 5 mg/kg of CNP or PEG-CNP was i.v. administered to the BALB/c mice. Two hours later, the mice were anesthetized and the hearts were perfused with saline followed by 4% paraformaldehyde. Tissues and tumors were removed for consecutive frozen sections of 10 μm thickness preparation. Nuclei were stained with PI for 5 min. The distribution of fluorescence was observed by a confocal microscope (LSM710, Carl Zeiss, Germany).

AUTHOR INFORMATION

Corresponding Author

*Fax: 86 28 85502532; Tel: 86 28 85502575; E-mail: gaohuile@scu.edu.cn.

Notes

The authors declare no competing financial interest.

ACKNOWLEDGMENTS

The work was funded by the Sichuan University Starting Foundation for Young Teachers (2014SCU11044) and National Natural Science Foundation of China (81373337).

REFERENCES

(1) Wu, P., and Yan, X. P. (2013) Doped quantum dots for chemo/biosensing and bioimaging. *Chem. Soc. Rev. 42*, 5489−521.

(2) Cao, L., Wang, X., Meziani, M. J., Lu, F., Wang, H., Luo, P. G., Lin, Y., Harruff, B. A., Veca, L. M., Murray, D., Xie, S. Y., and Sun, Y. P. (2007) Carbon dots for multiphoton bioimaging. *J. Am. Chem. Soc. 129*, 11318−9.

(3) Li, W., Zhang, Z., Kong, B., Feng, S., Wang, J., Wang, L., Yang, J., Zhang, F., Wu, P., and Zhao, D. (2013) Simple and green synthesis of nitrogen-doped photoluminescent carbonaceous nanospheres for bioimaging. *Angew. Chem., Int. Ed. Engl. 52*, 8151−5.

(4) Baker, S. N., and Baker, G. A. (2010) Luminescent carbon nanodots: emergent nanolights. *Angew. Chem., Int. Ed. Engl. 49*, 6726−44.

(5) Cao, L., Meziani, M. J., Sahu, S., and Sun, Y. P. (2013) Photoluminescence properties of graphene versus other carbon nanomaterials. *Acc. Chem. Res. 46*, 171−80.

(6) Li, H., Kang, Z., Liu, Y., and Lee, S. (2012) Carbon nanodots: synthesis, properties and applications. *J. Mater. Chem. 22*, 24230−24253.

(7) Fang, Y., Guo, S., Li, D., Zhu, C., Ren, W., Dong, S., and Wang, E. (2012) Easy synthesis and imaging applications of cross-linked green fluorescent hollow carbon nanoparticles. *ACS Nano 6*, 400−9.

(8) Kong, B., Zhu, A., Ding, C., Zhao, X., Li, B., and Tian, Y. (2012) Carbon dot-based inorganic-organic nanosystem for two-photon imaging and biosensing of pH variation in living cells and tissues. *Adv. Mater. 24*, 5844−8.

(9) Yang, Y., Cui, J., Zheng, M., Hu, C., Tan, S., Xiao, Y., Yang, Q., and Liu, Y. (2012) One-step synthesis of amino-functionalized fluorescent carbon nanoparticles by hydrothermal carbonization of chitosan. *Chem. Commun. (Camb.) 48*, 380−2.

(10) Sahu, S., Behera, B., Maiti, T. K., and Mohapatra, S. (2012) Simple one-step synthesis of highly luminescent carbon dots from orange juice: application as excellent bio-imaging agents. *Chem. Commun. (Camb.) 48*, 8835−7.

(11) Ruenraroengsak, P., Cook, J. M., and Florence, A. T. (2010) Nanosystem drug targeting: Facing up to complex realities. *J. Controlled Release 141*, 265−76.

(12) Vega-Villa, K. R., Takemoto, J. K., Yanez, J. A., Remsberg, C. M., Forrest, M. L., and Davies, N. M. (2008) Clinical toxicities of nanocarrier systems. *Adv. Drug Delivery Rev. 60*, 929−38.

(13) Du, F., Ming, Y., Zeng, F., Yu, C., and Wu, S. (2013) A low cytotoxic and ratiometric fluorescent nanosensor based on carbon-dots for intracellular pH sensing and mapping. *Nanotechnology 24*, 365101.

(14) Harris, J. M., and Chess, R. B. (2003) Effect of pegylation on pharmaceuticals. *Nat. Rev. Drug Discovery 2*, 214−21.

(15) Kurata, A., Kawaguchi, N., Kido, T., Inoue, K., Suzuki, J., Ogimoto, A., Funada, J., Higaki, J., Miyagawa, M., Vembar, M., and Mochizuki, T. (2013) Qualitative and quantitative assessment of adenosine triphosphate stress whole-heart dynamic myocardial perfusion imaging using 256-slice computed tomography. *PLoS One 8*, e83950.

(16) Knuuti, J., Bengel, F., Bax, J. J., Kaufmann, P. A., Le Guludec, D., Perrone, F. P., Marcassa, C., Ajmone, M. N., Achenbach, S., Kitsiou, A., Flotats, A., Eeckhout, E., Minn, H., Hesse, B. (2013) Risks and benefits of cardiac imaging: an analysis of risks related to imaging for coronary artery disease *Eur. Heart J.* Published Online December 29, 2013 10.1093/eurheartj/eht512.

(17) Owens, D. R., and Peppas, N. A. (2006) Opsonization, biodistribution, and pharmacokinetics of polymeric nanoparticles. *Int. J. Pharm. 307*, 93−102.

(18) Walkey, C. D., Olsen, J. B., Guo, H., Emili, A., and Chan, W. C. (2012) Nanoparticle size and surface chemistry determine serum protein adsorption and macrophage uptake. *J. Am. Chem. Soc. 134*, 2139−47.

(19) Zhu, S., Meng, Q., Wang, L., Zhang, J., Song, Y., Jin, H., Zhang, K., Sun, H., Wang, H., and Yang, B. (2013) Highly photoluminescent carbon dots for multicolor patterning, sensors, and bioimaging. *Angew. Chem., Int. Ed. Engl. 52*, 3953−7.

(20) Pan, D., Zhang, J., Li, Z., Wu, C., Yan, X., and Wu, M. (2010) Observation of pH-, solvent-, spin-, and excitation-dependent blue

photoluminescence from carbon nanoparticles. *Chem. Commun. (Camb.) 46*, 3681−3.
(21) Sevilla, M., and Fuertes, A. B. (2009) Chemical and structural properties of carbonaceous products obtained by hydrothermal carbonization of saccharides. *Chem.—Eur. J. 15*, 4195−4203.
(22) Liu, S., Tian, J., Wang, L., Zhang, Y., Qin, X., Luo, Y., Asiri, A. M., Al-Youbi, A. O., and Sun, X. (2012) Hydrothermal Treatment of Grass: A Low-Cost, Green Route to Nitrogen-Doped, Carbon-Rich, Photoluminescent Polymer Nanodots as an Effective Fluorescent Sensing Platform for Label-Free Detection of Cu(II) Ions. *Adv. Mater. 24*, 2037−2041.
(23) Dufort, S., Sancey, L., and Coll, J. L. (2012) Physico-chemical parameters that govern nanoparticles fate also dictate rules for their molecular evolution. *Adv. Drug Delivery Rev. 64*, 179−89.
(24) Aggarwal, P., Hall, J. B., McLeland, C. B., Dobrovolskaia, M. A., and McNeil, S. E. (2009) Nanoparticle interaction with plasma proteins as it relates to particle biodistribution, biocompatibility and therapeutic efficacy. *Adv. Drug Delivery Rev. 61*, 428−37.
(25) Gao, H., and He, Q. (2014) The interaction of nanoparticles with plasma proteins and the consequent influence on nanoparticles behavior. *Expert Opin. Drug Delivery 11*, 409−20.
(26) Zhang, R., Liu, Y., Yu, L., Li, Z., and Sun, S. (2013) Preparation of high-quality biocompatible carbon dots by extraction, with new thoughts on the luminescence mechanisms. *Nanotechnology 24*, 225601.
(27) Liu, Y. F., and Yu, J. S. (2010) In situ synthesis of highly luminescent glutathione-capped CdTe/ZnS quantum dots with biocompatibility. *J. Colloid Interface Sci. 351*, 1−9.
(28) Durgadas, C. V., Sreenivasan, K., and Sharma, C. P. (2012) Bright blue emitting CuSe/ZnS/silica core/shell/shell quantum dots and their biocompatibility. *Biomaterials 33*, 6420−9.
(29) Yamada, Y., and Harashima, H. (2008) Mitochondrial drug delivery systems for macromolecule and their therapeutic application to mitochondrial diseases. *Adv. Drug Delivery Rev. 60*, 1439−62.
(30) Almeida, J. P., Chen, A. L., Foster, A., and Drezek, R. (2011) In vivo biodistribution of nanoparticles. *Nanomedicine (London) 6*, 815−35.
(31) Lankveld, D. P., Rayavarapu, R. G., Krystek, P., Oomen, A. G., Verharen, H. W., van Leeuwen, T. G., De Jong, W. H., and Manohar, S. (2011) Blood clearance and tissue distribution of PEGylated and non-PEGylated gold nanorods after intravenous administration in rats. *Nanomedicine (London) 6*, 339−49.
(32) Sher, T., and Gertz, M. A. (2014) Recent advances in the diagnosis and management of cardiac amyloidosis. *Future Cardiol. 10*, 131−46.